Similarities and differences between direct current and radio-frequency glow discharges: a mathematical simulation†

Invited Lecture

JAAS

Full Paper

Annemie Bogaerts* and Renaat Gijbels

Department of Chemistry, University of Antwerp, Universiteitsplein 1, B-2610 Wilrijk-Antwerp, Belgium

Received 18th January 2000, Accepted 28th February 2000
Published on the Web 22nd March 2000

A comprehensive three-dimensional modeling network has been developed both for argon glow discharges operating in the direct current (dc) and in the radio-frequency (rf) mode. The model network consists of various Monte Carlo, fluid and collisional–radiative models to describe the behavior of the electrons, argon atoms, argon ions, fast argon atoms, argon atoms in various excited levels, sputtered copper atoms and the corresponding ions, both in the ground state and in various excited levels. Typical results of the simulations comprise the electrical characteristics of the glow discharge, the densities, fluxes and energies of the various plasma species, information about collisions in the plasma, optical emission intensities and erosion rates due to sputtering. The results for the dc and the rf discharges have been compared. It is found that for the same input power (*i.e.*, power effectively going into the plasma) and pressure, the rf discharge requires lower voltages than the dc discharge, in agreement with experimental data. The erosion rates and optical emission intensities are, however, rather similar in both operation modes, which is also in agreement with experiment.

1 Introduction

Although direct current (dc) glow discharges are still commonly used in analytical spectrometry, interest is also shifting to radio-frequency (rf) discharges, mainly because they allow the direct analysis of non-conducting materials, and, therefore, they widen the application field of glow discharge mass spectrometry (GDMS) and optical emission spectrometry (GD-OES) to a larger variety of sample types. In order to obtain a better understanding of the operating principles of rf and dc glow discharges, we have developed a hybrid modeling network, consisting of Monte Carlo, fluid and collisional–radiative models for the various plasma species. Such a model network has initially been developed for a dc discharge,[1] and more recently been adapted to an rf discharge. After a brief description of the model network, the present paper will mainly deal with a comparison of the calculation results obtained for a dc and an rf discharge, and we will check this with experimental data when available.

2 Description of the model network

The species assumed to be present in the plasma and considered in the model network are argon atoms, argon ions, fast argon atoms created from the argon ions by collisions, argon atoms in various excited levels, electrons, sputtered copper atoms and the corresponding copper ions, in the ground state and also in various excited levels. These plasma species are described by a combination of Monte Carlo, fluid and collisional–radiative models, depending on the type of species, because each of the models has its specific advantages and drawbacks. Indeed, the Monte Carlo method is very accurate, since it describes the particles on the lowest microscopic level without equilibrium assumptions; however, it requires a long computation time, especially for "slow" plasma species, because a large number of particles has to be followed to yield satisfactory statistics. The fluid approach, on the other hand, which is based on the continuity and transport equations, is considerably faster. However, since it treats the species as a continuum in equilibrium with the electric field, it is not valid for "fast" plasma species, which gain more energy from the electric field than they lose locally by collisions. Therefore, we use a Monte Carlo model for the fast plasma species: fast electrons in the entire discharge; argon ions and fast argon atoms; and copper ions in the cathode sheath (or cathode dark space; this is the region adjacent to the cathode, characterized by a strong electric field). We use a fluid model for the slow plasma species, like slow electrons and argon ions in the bulk plasma (or negative glow: *i.e.*, the main part of the discharge, with a very weak electric field). Moreover, a collisional–radiative model is applied for the argon atoms and copper atoms and ions in various excited levels. This is a kind of fluid model, consisting of a set of balance equations (one for each electron energy level), with different production and loss processes. These processes are either collisional or radiative, hence the name of this model.

All the models are coupled to each other, due to the interaction processes between the species, and they are solved iteratively until final convergence is reached. This generally takes several days. The Monte Carlo models are developed in three dimensions, whereas, for the fluid and collisional–radiative models, two dimensions are sufficient, due to the cylindrical symmetry of the discharge cell under study (see below). An overview of the various species, as well as the models used to describe them, is presented in Table 1. In the following, a brief description of each of the sub-models will be given.

2.1 Monte Carlo model for fast electrons

A large number of electrons, emitted from the rf electrode (or cathode) or created by ionization collisions in the sheath, are followed one after the other, as a function of time. During successive time-steps, their trajectory is calculated by Newton's

†Presented at the 2000 Winter Conference on Plasma Spectrochemistry, Fort Lauderdale, FL, USA, January 10–15, 2000.

DOI: 10.1039/b000519n

Table 1 Overview of the various plasma species considered in the model network, and the models used to describe these species, together with references for more detailed information

Plasma species	Model	Ref. (dc)	Ref. (rf)
Argon atoms	No model; assumed to be at rest	—	—
Fast electrons	Monte Carlo model	2	3, 4
Slow electrons	Fluid model	5	3, 4
Argon ions	Fluid model	5	3, 4
Argon ions in sheath	Monte Carlo model	6	7
Fast argon atoms in sheath	Monte Carlo model	6	7
Argon atoms in various excited levels	Collisional–radiative model	8	9
Thermalization of sputtered copper atoms	Monte Carlo model	10	12
Copper atoms and ions in excited levels	Collisional–radiative model	11	12
Copper ions in sheath	Monte Carlo model	11	12

laws, and their collisions (*i.e.*, occurrence of a collision, kind of collision, and new energy and direction after the collision) are treated with random numbers. By following, in this statistical way, a large number of electrons, their behavior can be simulated. The electrons are followed as a function of time, until (periodic) steady state is reached (which happens in the rf case already after two rf cycles) or until the electrons are transferred to the slow electron group. Indeed, when the electrons arrive in the bulk plasma, and have energies below the threshold for inelastic collisions (which is about 12 eV for argon excitation), they are not important as fast electrons anymore, because they will only play a role in carrying electrical current and in providing negative space charge. Therefore, they will be transferred to the slow electron group in the bulk plasma, which will be followed with the fluid model (see below). More details about this Monte Carlo model can be found, *e.g.*, in ref. 2 for the dc model, and in refs. 3 and 4 for the rf model.

2.2 Fluid model for the slow electrons and argon ions

The slow electrons are studied with a fluid model, together with the argon ions. The equations are the continuity equations for slow electrons and argon ions, the transport equations (based on diffusion and on migration in the electric field) for electrons and ions, and Poisson's equation, to obtain a self-consistent electric field distribution from the electron and ion densities. The equations are strongly coupled and solving them is a difficult numerical task; in fact, this model is the most difficult one to solve in the entire modeling network.

It should be mentioned that an important difference arises in this fluid model for the dc and the rf discharge. Indeed, in the dc discharge, the electrons, which are transferred to the slow electron group in the bulk plasma (negative glow), do really remain slow, because the bulk electric field is rather weak. In the rf discharge, on the other hand, the electrons which are slowed down can be heated again by the oscillating rf electric field in the bulk plasma, and they can again give rise to inelastic collisions. Therefore, an additional equation is used in the rf fluid model (*i.e.*, an energy balance equation), to calculate the electron mean energy. From this mean energy, the rate of ionization produced by the "heated slow electrons" is calculated. This ionization, produced by electrons heated in the bulk plasma by the oscillating electric field, is called "α-ionization". On the other hand, the ionization due to electrons emitted from the cathode (or rf electrode) and due to the ones created from these emitted electrons, which gain energy during their travel through the cathode sheath, is called "γ-ionization". It has been demonstrated that α-ionization (calculated in the fluid model) is more important than γ-ionization (calculated in the Monte Carlo model) for the conditions under study.[4] In the dc case, only γ-ionization comes into play, and this explains why the rf discharge requires lower voltages than the dc discharge, for the same pressure and power (see below). For more detailed information about the dc and rf fluid model, we refer to refs. 5 and refs. 3 and 4, respectively.

2.3 Monte Carlo model for the argon ions and fast argon atoms in the cathode sheath

Because the fluid model assumes that the plasma species are in equilibrium with the electric field, it is not very suitable to be used in the sheath, where the charged plasma species (ions, electrons) are not in equilibrium with the strong electric field. Therefore, the ions are described in this sheath region not only with a fluid model, but also with a Monte Carlo model. The principle is the same as for the fast electron Monte Carlo model (see above). Moreover, the fast argon atoms, created from elastic collisions (both with isotropic scattering and forward scattering, as an approximation to charge transfer) from the argon ions, are also treated with a Monte Carlo model in the sheath region. Further details about this argon ion and fast argon atom Monte Carlo model can be found in refs. 6, 7 for the dc and the rf case, respectively.

2.4 Collisional–radiative model for the argon excited levels

Sixty-four excited argon levels are taken into account in this model; some of them are individual levels (*e.g.*, the 4s levels) but most of them are effective levels, consisting of several individual levels with similar excitation energy and quantum numbers. For each of the levels, a balance equation is constructed with different populating and depopulating processes. The processes taken into account in this model are electron, argon ion and atom impact ionization, excitation, de-excitation as well as three-body recombination, radiative recombination and radiative decay between all levels, and Hornbeck–Molnar associative ionization for the levels with excitation energy above 14.71 eV. Moreover, for the 4s levels, some additional processes are incorporated, like Ar*–Ar* (associative) ionization, Penning ionization of sputtered copper atoms, three-body collisions with argon atoms, and radiation trapping for the resonant levels, which radiate to the argon ground state. More information is given elsewhere for the dc case[8] and the rf case.[9]

2.5 Monte Carlo model for the thermalization of the sputtered copper atoms

When the copper atoms are sputtered from the cathode (or rf electrode), they have energies in the order of 5–10 eV, which they lose almost immediately by collisions with the argon gas atoms, until they are thermalized. This thermalization process occurs almost "immediately", and it is finished before the diffusion starts. Therefore, both processes are separated in time, and they can be described by two separate models. The thermalization process is described with a Monte Carlo model, similar to the electron Monte Carlo model.[10] Output of this model is the so-called thermalization profile (*i.e.*, distribution of thermalized copper atoms as a function of distance from the

electrode), which serves as initial distribution for the diffusion of the thermalized copper atoms, described in the next model.

2.6 Collisional-radiative model for the copper atoms and ions in the ground state and in various excited levels

As mentioned above, the further transport of the thermalized copper atoms occurs by diffusion. Moreover, the copper atoms can become excited and/or ionized. The behavior of the copper atoms and ions, both in the ground state and in excited levels, is described with a collisional–radiative model. Eight Cu^0 atomic levels, seven Cu^+ ionic levels, as well as the Cu^{++} levels are incorporated in the model. Most of the levels are again a combination of several individual levels with similar excitation energy and quantum numbers. Transport occurs by diffusion for the atoms, and by diffusion and migration in the electric field for the ions. Sixteen balance equations (one for each level) describe the production and loss processes for the various levels. The processes taken into account are electron and atom impact ionization, excitation, de-excitation and radiative decay for each of the levels, three-body electron-ion recombination to the highest excited levels, as well as Penning ionization by argon metastable atoms and asymmetric charge transfer with argon ions, for some specific levels. Detailed descriptions for the dc and the rf model, are available.[11,12]

2.7 Monte Carlo model for the copper ions in the sheath

In analogy to the argon ions, the copper ions are not in equilibrium with the strong electric field in the sheath, and they are, therefore, also described with a Monte Carlo model in this region. This model is very similar to the Monte Carlo model for argon ions. It should be mentioned that the Monte Carlo models for the argon ions, fast argon atoms and copper ions in the sheath region are especially important to calculate the energy distributions of these species bombarding the cathode (or rf electrode) which are needed to calculate the amount of sputtering.

3 Results and discussion

3.1 Electrical characteristics

The calculations are performed for representative experimental conditions such as used by Hoffmann[13] in a Grimm-type glow discharge source with a 4 mm anode diameter. We have, however, simplified the Grimm-cell geometry by assuming a simple cylinder with a diameter of 4 mm and a length of 2 cm. This is justified since the discharge is most intense in the region close to the sample (rf electrode or cathode). The discharge conditions measured by Hoffmann[13] were a gas pressure of 5 Torr and an electrical power of about 38 W, both for the dc and the rf mode, in order to make a direct comparison between both operation modes possible. We will perform our calculations at the same conditions. The measured electrical characteristics, such as the electrical power, the rf and dc bias voltage, can then be used to check our calculated results.

Fig. 1 shows the calculated potential at the rf electrode, as a function of time in the rf-cycle (thick solid line). We assumed a purely sinusoidal waveform, although the output of most rf generators deviates from this perfect sine-form, due to the superposition of higher order waveforms. However, the rf generator used to produce the experimental data[13] was sinusoidal within 10%. It appears from Fig. 1 that the potential at the rf electrode is negative during most of the rf cycle; it becomes only positive around $\omega t = \pi/2$. The reason for this is the highly negative calculated dc-bias voltage (−519 V; solid line), which arises from the large difference in size of the rf powered and grounded electrodes in the Grimm-type source, in combination with the capacitive coupling

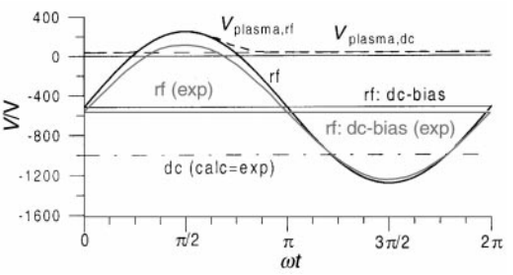

Fig. 1 Calculated potential at the rf electrode, as a function of time in the rf cycle (thick solid line) and calculated rf dc-bias, as well as the measured values (grey lines). Also shown are the calculated and measured voltages in the dc case (dash-dotted line), and the calculated plasma potential in the rf and the dc case (broken line).

between the two electrodes. The experimental potential at the rf electrode, as a function of time in the rf cycle, is also presented in Fig. 1, as well as the measured dc-bias voltage (grey curves). The calculated and measured dc-bias voltages appear to be in satisfactory agreement (*i.e.*, −519 V for the calculated, and −569 V for the measured value). The amplitude of the potential at the rf electrode was calculated to be somewhat higher than the experimental result (*i.e.*, 769 V compared to 680 V), but the general waveforms look very similar to each other.

Also presented in Fig. 1 are the calculated and measured voltages in the dc mode. It should be mentioned that the rf and dc models are essentially different in the types of input and output parameters. Indeed, in the rf model, the power and pressure are given as input, and the voltage and current as a function of time in the rf cycle, as well as the dc-bias voltage, are calculated. In the dc model, on the other hand, the voltage and pressure are used as input values, and the electrical current, and from this also the power, is calculated. In the present investigation we want to make a comparison at the same values of pressure and power. Therefore, we had to find out in the dc model which voltage value yielded an electrical power of about 38 W. We found a value of 1000 V, which is in excellent agreement with the experimental value (see Fig. 1: dash-dotted black line). Hence, it follows that, for the same power and pressure, the rf mode yields much lower voltages than the dc mode. The reason for this is the more efficient electron impact ionization in the rf mode, due to the oscillating electric field (see also below).

In spite of the higher voltage in the dc mode, the plasma potential is very similar in both operation modes, as is illustrated in Fig. 1 (dashed curves). In the rf case, it reaches a maximum of about 250 V (*i.e.*, equal to the potential at the rf electrode) around $\omega t = \pi/2$, but then it drops, and most of the time (*i.e.*, in the beginning and in the second half of the rf cycle) it is around 36–37 V, which is also the value of the dc plasma potential.

The calculated rf electrical current is plotted as a function of time in the rf cycle in Fig. 2, as well as the various contributions to the rf current

$$j_{rf,total}(t) = j_{rf,ion}(t) - j_{rf,elec}(t) + j_D(t).$$

Here, $j_{rf,total}$ is the total rf current flowing in the plasma (negative sign when it is directed toward the rf electrode, and positive sign when it is directed away from the rf electrode); $j_{rf,ion}$ is the ion current [which contributes with a positive sign to the total electrical current in the plasma, due to the positive charge of the ions (it is always negative, because the ions are always directed toward the rf electrode)]; $j_{rf,elec}$ is the electron current (which contributes with a negative sign to the total electrical current in the plasma, due to its negative charge); and j_D is the displacement current. The latter is typical for rf

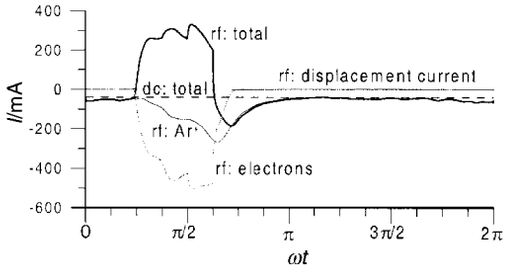

Fig. 2 Calculated rf current as a function of time in the rf cycle (thick solid line), as well as the contributions of argon ion, electron and displacement current (thin solid lines), and the dc current (broken line).

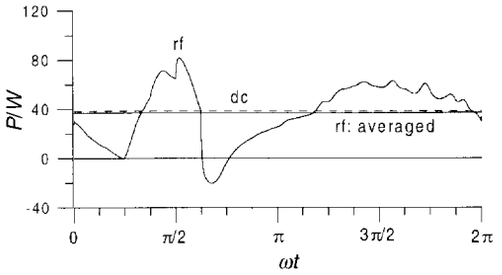

Fig. 3 Calculated power in the rf case (as a function of time in the rf cycle, and the time-averaged value; solid lines) and in the dc case (broken line).

discharges, and arises due to the movement of the rf sheath as a function of time. It is calculated as:[3]

$$j_D = \varepsilon_0 \frac{\partial E}{\partial t}$$

where ε_0 is the permittivity in vacuum, E is the electric field strength at the rf electrode and t stands for the time. Indeed, the rf sheath is characterized by a positive space charge (see below). Since the sheath changes in thickness[3] during the rf cycle, and since the argon ion density remains constant (see below), the total positive space charge in the sheath changes in time. Since $I = dq/dt$ (where I is the electrical current and q is the electrical charge) this gives rise to a current, called "displacement current". It is, however, obvious from Fig. 2 that the displacement current has a negligible contribution to the total current, for the discharge conditions under study. Indeed, this type of current is typical for rf discharges with electrodes of comparable size, when the rf sheaths change considerably. At lower gas pressures and lower dc bias voltages, the displacement current is (in the rf sheath) generally of comparable magnitude or even higher than the ion or electron currents.[14,15] Since the Grimm-type cell under study here gives rise to a large dc bias (see above) so that the positive ion sheath is present most of the time in front of the rf electrode, it resembles a dc discharge, where the displacement current is absent.

During most of the rf cycle, the electrical current at the rf electrode is primarily carried by the ions bombarding the electrode (negative sign), as analogy to a dc discharge. When these ions strike the rf electrode, they may induce current flow through the power supply, by (1) ejecting a secondary electron from the electrode surface and (2) acquiring an electron as they are neutralized. Both mechanisms are taken into account in our model. Around $\omega t = \pi/2$, where the electrode potential is positive, a large electron flux also hits the rf electrode, due to the lower mass, and hence higher mobility of the electrons. The electron current has also a negative sign here, giving rise to a positive total rf current (see Fig. 2). Integrated over the entire rf cycle, the total rf current at the rf electrode is zero, which is imposed by the capacitive rf coupling of the electrodes.

Also illustrated in Fig. 2 is the total dc current at the cathode (broken line), which is of course constant in time. In general, it is comparable in magnitude to the total rf current; only around $\omega t = \pi/2$, where the rf current is due to a large electron flux, the dc current is considerably lower than the total rf current.

By multiplying the values of potential and electrical current at the rf electrode or cathode, the electrical power is obtained. It should be mentioned that the terms "power" and "input power" are used in this paper for the "effective plasma power", *i.e.*, the input power that really goes into the plasma. In the rf case, this is generally not the same as the power that is generated from the rf supply. Indeed, it is well known that a substantial part (typically 20–60%) of the latter power is lost in cables, connectors, *etc.* before reaching the plasma. The electrical power is presented, for both the rf case (as a function of time in the rf cycle) and the dc case, in Fig. 3. The time evolution of the rf power is in good agreement with experimental data.[16] Also the time-averaged rf power is shown in Fig. 3; it is more or less equal to the dc power. These power values were used as input in the models (see above), to compare with the experimental data[13] [*i.e.*, input power or effective plasma power: $P = 37$ W (rf) and 38 W (dc)]. The figure shows that the power calculated from the product of calculated voltage and current is indeed equal to the input power, for both the dc and the rf case.

3.2 Potential distributions

Fig. 4 illustrates the two-dimensional potential distributions throughout the discharge, at four different times in the rf cycle, as well as in the dc discharge. The rf electrode or cathode is found at the left-hand side of the figure. At $\omega t = \pi/2$ [Fig. 4(a)] the potential is positive (*ca.* 250 V) at the rf electrode, and it decreases very slowly to zero at the grounded cell walls. There is a strong sheath in front of the grounded electrode, especially in the vicinity of the rf electrode, as appears from the steep potential gradient there. Hence, the electric field ($E = -\nabla$ V) will be very low in the region adjacent to the rf electrode, but it will be considerable in the bulk plasma and close to the grounded electrode, at this time in the rf cycle.

The situation is completely different at the other times in the rf cycle [Fig. 4(b–d)]. Indeed, the potential here is strongly negative at the rf electrode (*i.e.*, about -520 V at $\omega t = 0$, π and 2π, and almost -1300 V at $\omega t = 3\pi/2$); it increases rapidly in the rf sheath till zero at the end of the sheath. The rf sheath is about 0.6 mm long around $\omega t = 3\pi/2$ and about 0.4 mm at $\omega t = 0$ and π. The potential reaches positive values in the bulk plasma, called the "plasma potential". The plasma potential varies between 36 V at $\omega t = \pi$ and $3\pi/2$ and *ca.* 50 V at $\omega t = 2\pi$. Finally, the potential returns to zero at the grounded cell walls. This potential distribution gives rise to a strong electric field in the rf sheath and a very weak electric field in the bulk plasma.

The rf potential distributions in Fig. 4(b–d) resemble very much the dc potential distribution, presented in Fig. 4(e), which is also very negative (*i.e.*, -1000 V) at the cathode, crosses the zero-line at about 0.7 mm from the cathode, and reaches positive values of 36 V in the bulk plasma. Hence, except around $\omega t = \pi/2$ when the potential at the rf electrode is positive, the potential distributions and electric fields are comparable to each other in the dc and the rf discharge.

3.3 Densities of the plasma species

The calculated two-dimensional density profiles of the argon ions throughout the discharge, in both the dc and the rf discharge, are presented in Fig. 5. The rf ion density is more or less constant throughout the entire rf cycle, since the ions cannot follow the rapidly oscillating electric field due to their high mass and hence low mobility. Both the dc and rf density are low and rather constant in the rf sheath, and they reach a maximum of about 10^{13} cm^{-3} at 2 mm from the electrode. The rf ion density drops, however, more slowly to low values as a

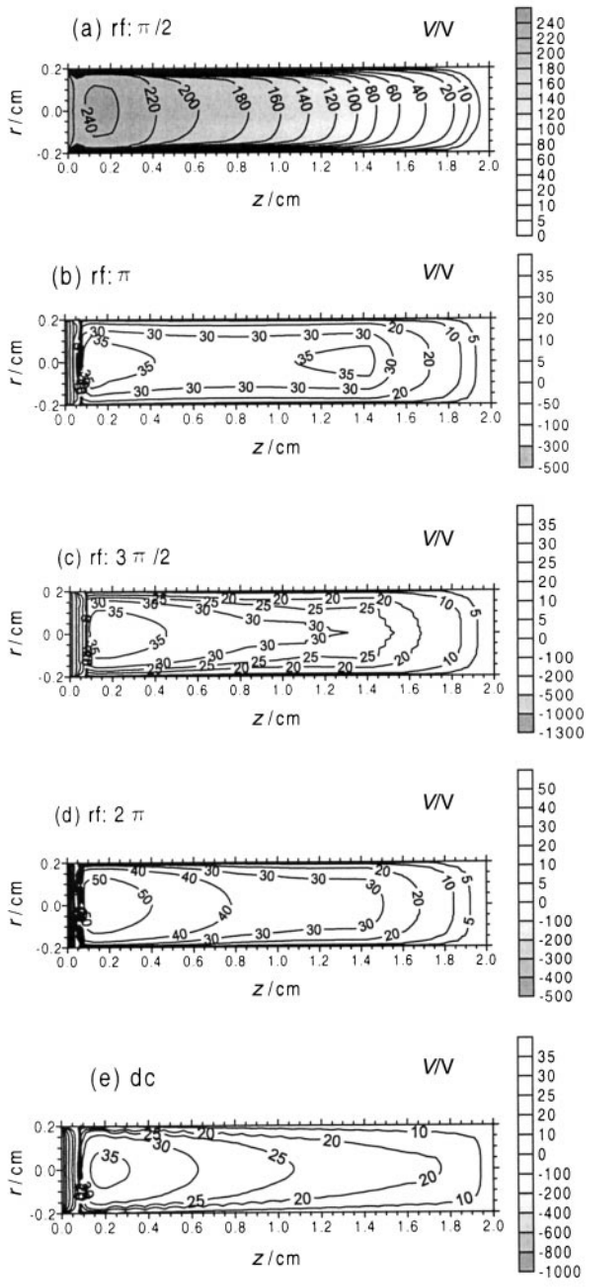

Fig. 4 Calculated two-dimensional potential distributions in the rf case, at four different times in the rf cycle (a–d) and in the dc case (e). The rf electrode (or cathode) is found at the left end of the figure.

function of distance from the electrode than the dc ion density, so that it can be concluded that, in the rf case, the discharge cell is more filled with argon ions than in the dc case. The electron density (not shown here) is more or less equal to the argon ion density in the plasma bulk, both in the dc and the rf case, giving rise to nearly charge neutrality and hence a low electric field.[4] The same is true for the rf sheath at $\omega t = \pi/2$, where the electric field is also low (or the potential nearly constant). However, at the other times in the rf cycle, the electron density returns to zero in the rf sheath,[4] resulting in a positive space charge and hence a high electric field (or large potential drop; see Fig. 4).

Electron and argon ion densities have been measured with a Langmuir probe in Marcus' group, for both a dc[17,18] and an rf[19] discharge. The obtained density values were several orders of magnitude lower than our results (*i.e.*, order of 10^{11} cm^{-3} and 10^{10} cm^{-3} for the dc and the rf discharge, respectively). However, as far as we understand from their papers, the experimental discharge conditions were lower than the ones under investigation here, and were also not the same for the dc and the rf mode. We have calculated with our dc models that the electron and ion densities can indeed vary over several orders of magnitude for different discharge conditions and cell geometries (*e.g.*, $\approx 10^{11}$ cm^{-3} at 0.5 Torr, 1000 V, 2 mA in the VG9000 cell,[20] and $\approx 10^{13}$ cm^{-3} at 4 Torr, 800 V, 30 mA in a Grimm-type cell[21]). In future work, we would like to make a detailed comparison with the experimental Langmuir probe results, for exactly the same discharge conditions and source design.

Fig. 6 shows the calculated two-dimensional density profiles of the argon atoms in the metastable (4s $[3/2]_2$) level, in both the rf and the dc case. Again, the metastable densities appear to be constant in time throughout the entire rf cycle. Looking at the absolute values, the metastable densities are characterized by similar peak values in both the dc and the rf mode. The location of the peaks is, however, slightly different. Indeed, the rf metastable density shows a pronounced maximum near the rf electrode, attributed to electron, but also fast argon ion and atom impact excitation, and it has also rather high values in the entire bulk plasma, especially between 1.2 and 1.6 cm from the rf electrode. The latter is due to excitation by heated slow electrons (or α-electrons) around $\omega t = \pi/2$. Indeed, due to the non-negligible electric field in the bulk plasma around $\omega t = \pi/2$ [see *e.g.*, Fig. 4(a)], the electrons can become slightly heated, and they have just enough energy to cause excitation and ionization. The rather large amount of ionization in the bulk plasma around $\omega t = \pi/2$ (see also below), on one hand, is responsible for the lower voltages in the rf mode compared to the dc mode (at the same power and gas pressure). The considerable amount of excitation, on the other hand, results in rather high values of the metastable density in the bulk plasma. The dc metastable density is also characterized by a pronounced peak close to the cathode, again mainly due to electron, but also to fast argon ion and atom impact excitation, and it reaches a second, but clearly lower maximum in the bulk plasma between 0.8 and 1 cm from the cathode. This is also entirely due to electron impact excitation as in the rf case, but the peak is clearly lower and it is somewhat closer to the cathode, where the electrons have still enough energy for excitation. Indeed, in the dc mode, the bulk electric field is rather low, and the electrons cannot significantly become heated anymore as in the rf case around $\omega t = \pi/2$.

We have also calculated the level populations of higher excited argon levels. As an example, the one-dimensional density profiles of the $4p[1/2]_1$ level are illustrated in Fig. 7, at four different times in the rf cycle (black curves), as well as in the dc discharge (grey line). In contrast to the metastable density profiles, the $4p[1/2]_1$ level population changes slightly as a function of time in the rf cycle, because the higher excited (non-metastable) levels react more rapidly to the oscillating rf electric field. The $4p[1/2]_1$ level reaches a small peak adjacent to the rf electrode or cathode (due to fast argon ion and atom impact excitation), and a pronounced maximum at about 1–2 mm from the electrode (attributed to electron impact excitation), in both the rf case (at all times) and in the dc case. Further away from the electrode, in the bulk plasma, the density profiles are clearly different, both as a function of time in the rf cycle, and also in the dc discharge compared to the rf discharge. Indeed, the density is rather high at $\omega t = \pi/2$, where excitation due to α-electrons is appreciable, but it drops gradually at later times in the rf cycle, when the α-electrons lose their energy. In the dc discharge, the $4p[1/2]_1$ level population decreases much more rapidly in the bulk plasma, since the electrons do not have enough energy for excitation here. The higher excited levels show similar density distributions,[9] and are therefore not presented here. However, it was found[9] that

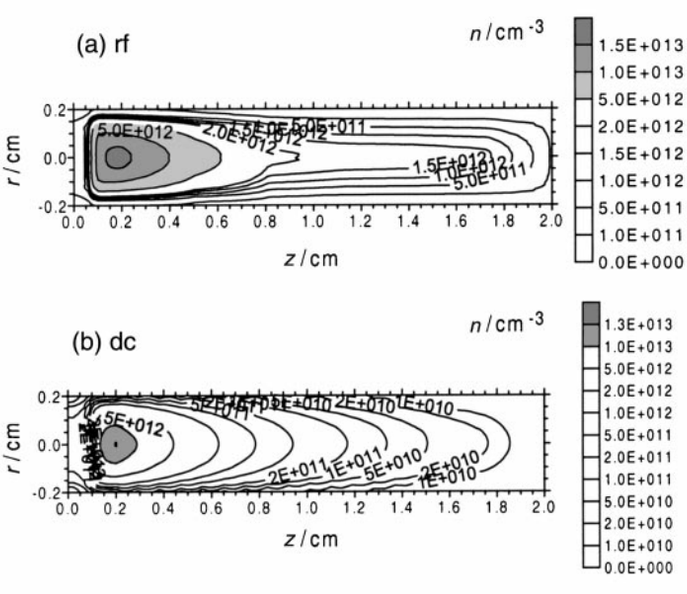

Fig. 5 Calculated two-dimensional density profiles of the argon ions, in the rf case (a) and the dc case (b).

the highly excited levels have a somewhat lower density at their maximum in the dc mode, compared to the rf mode, which suggests that excitation to these high levels is less efficient in the dc mode than in the rf mode.

Fig. 8 presents the calculated two-dimensional sputtered copper atom densities (in the ground state) in the rf (again found to be constant in time) and dc discharge. Only the first 4 mm adjacent to the sample are shown, because the densities at distances further away from the electrode become negligibly low. In both cases, the densities reach a maximum of about 5×10^{14} cm^{-3} very close to the electrode (at less than 0.5 mm). The maximum density in the dc case seems to be slightly higher than in the rf case, which is quite unexpected, since the erosion rate was found to be slightly lower (see further). However, the population levels of excited copper atoms are somewhat higher in the rf case,[12] and moreover, the density profile of the copper ground state atoms drops off more slowly in the rf discharge than in the dc case. In general, both density profiles look very similar.

The calculated density profiles of the Cu^+ ions in the ground state are also very similar in the rf and dc mode, both in relative profiles (*i.e.*, maximum around 1 mm) and even in absolute values (*ca.* 4×10^{11} cm^{-3}), as is illustrated in Fig. 9. The dc Cu^+ ion density reaches its maximum slightly further away from the cathode, and decreases more rapidly to low values at the cathode compared to the rf density, due to the somewhat longer length of the dc cathode sheath (*i.e.*, *ca.* 0.7 mm) compared to the rf sheath (varying between 0 and 0.6 mm; see Fig. 4). Nevertheless, the overall levels of the dc and rf Cu^+ ion densities are very similar. Moreover, we have found that the Cu^+ ions in excited levels are also characterized by similar level populations in both operation modes. This finding is not

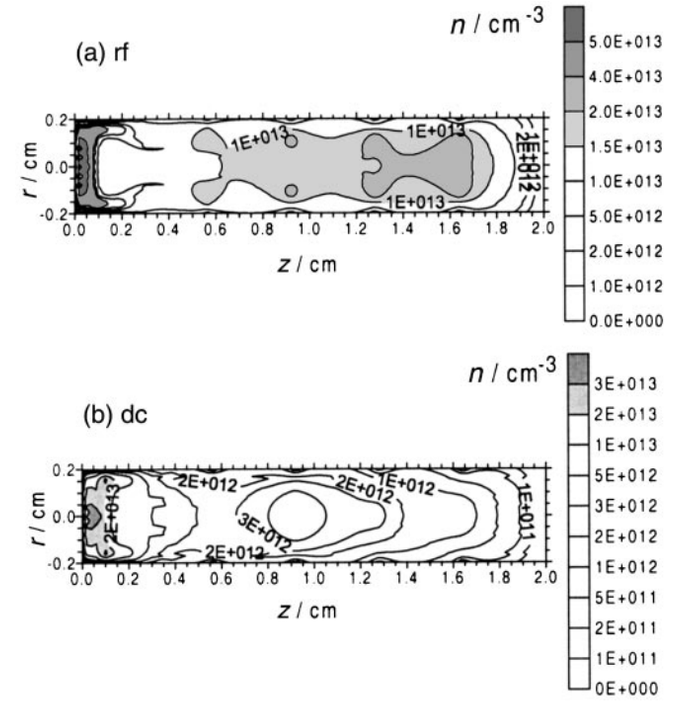

Fig. 6 Calculated two-dimensional density profiles of the argon metastable atoms (in the $4s[3/2]_2$ level), in the rf case (a) and the dc case (b).

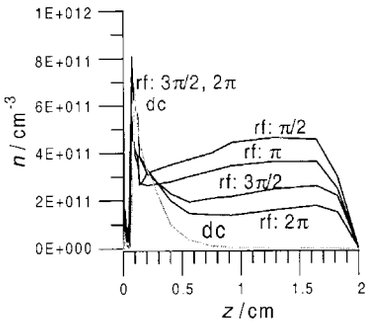

Fig. 7 Calculated one-dimensional density profiles of the argon excited atoms in the 4p $[1/2]_1$ level, in the rf case at four different times in the rf cycle (black lines) and in the dc case (grey line).

straightforward, taking into account the clear differences in electric potentials, currents and argon ion and electron densities in both discharge modes (see above). It turns out that, although the model predicts somewhat less efficient sputtering in the dc discharge, this appears to be compensated by slightly more efficient copper ionization. Finally, by comparing the absolute values of the Cu^+ ion densities at their maximum with the maximum density values of the copper atoms, the ionization degree could be estimated. It was found to be in the order of 0.1%, for both the rf and dc case.

The two-dimensional Cu^{++} ion density profiles, calculated for both the rf and the dc mode, are presented in Fig. 10. Again, the absolute values of the densities (*i.e.*, maximum of $3–4 \times 10^8$ cm^{-3}) and the relative shapes are nearly identical for both operation modes. Comparison of the absolute values of Fig. 10 with those of Fig. 9 shows that the estimated Cu^{++}/Cu^+ ratio is about 0.1%, hence similar to the Cu^+/Cu^0 ratio.

3.4 Information about collision processes in the plasma

The most important collision processes in the plasma are excitation and ionization. Excitation has already briefly been discussed in the previous section, when the argon metastable atom densities were presented. Moreover, the calculated relative contributions of the various populating and depopulating processes for the argon atom and copper atom and ion excited levels have been tabulated[9,12] for the discharge conditions under study here. In this section, we will focus on electron impact ionization in the plasma, because this process constitutes the major difference between rf and dc discharges.

In Fig. 11 the electron impact ionization rate of argon is plotted in one dimension as a function of distance from the rf electrode or cathode. As mentioned in Section 2, the ionization due to electrons is described, in the rf case, both in the Monte Carlo and in the fluid model. Indeed, the Monte Carlo model treats only the fast electrons, and once they are slowed down below the threshold for inelastic collisions in the bulk plasma, these electrons are transferred to the fluid model. However, these slow electrons can be heated again by the oscillating electric field (due to the movement of the rf sheath) and by the moderate electric field in the bulk plasma around $\omega t = \pi/2$ (see above, Fig. 4). Hence, these electrons can produce some more ionization, which is typical for an rf discharge, and is called "α-ionization". The ionization rates due to Monte Carlo electrons [*i.e.*, the electrons emitted by the rf electrode and the fast electrons created in collisions from the first group; (producing so-called "γ-ionization")] are presented, at four times in the rf cycle, at the top of Fig. 11. This type of ionization reaches a maximum at the sheath–bulk plasma interface. The ionization due to fluid electrons (α-ionization), which is shown at four times in the rf cycle in the middle part of Fig. 11, also reaches a maximum here at times $\omega t = \pi$, $3\pi/2$ and 2π. This maximum is caused by the electrons which are drawn towards the rf electrode around $\omega t = \pi/2$ and then accelerated back towards the bulk plasma at later times, when the rf sheath develops again and is characterized by a strongly negative electric field. It appears from Fig. 11(b) that the ionization at $\omega t = \pi$ is rather low compared to the other times. The reason is that the electrons, which have been drawn toward the rf electrode at $\omega t = \pi/2$, have not yet gained much energy on their way back to the bulk plasma at $\omega t = \pi$, to yield a lot of ionization. At later times ($\omega t = 3\pi/2$ and 2π), they have gained already enough energy to cause more ionization, giving rise to higher peaks in Fig. 11(b). The fluid ionization at $\omega t = \pi/2$ (presented by the broken line in the middle part of the figure) is characterized by a peak adjacent to the rf electrode (caused by the electrons drawn towards the rf electrode) and a broad maximum in the entire bulk plasma (caused by electrons accelerated here by the moderate electric field). The latter broad maximum corresponds with the rather high values of the argon metastable density in the bulk plasma, as has been explained before. The lower part of Fig. 11 presents the electron impact ionization rate in the dc case (*i.e.*, also γ-ionization). It reaches also a maximum at the sheath–negative glow interface, similar to the γ-ionization in the rf case, and is somewhat higher in magnitude than the time-averaged rf γ-ionization. However, in the dc case, no α-ionization takes place, so that the overall dc ionization is lower than the overall rf ionization, necessitating a higher dc voltage for the same conditions of pressure and power, in agreement with experiment (see above in Section 3.1).

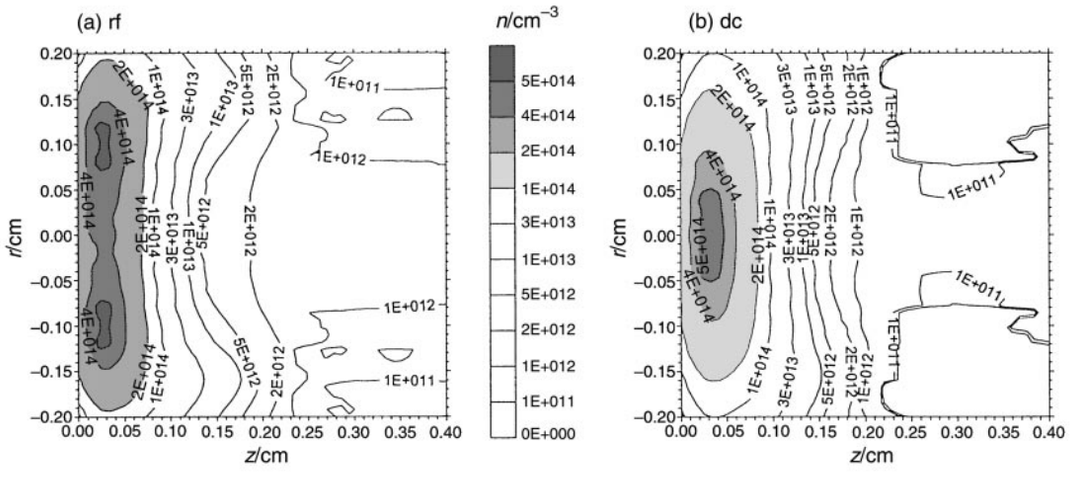

Fig. 8 Calculated two-dimensional density profiles of the sputtered copper atoms, in the rf case (a) and the dc case (b). Only the first 4 mm from the electrode are shown. Reprinted from ref. 12, with permission of Elsevier Science.

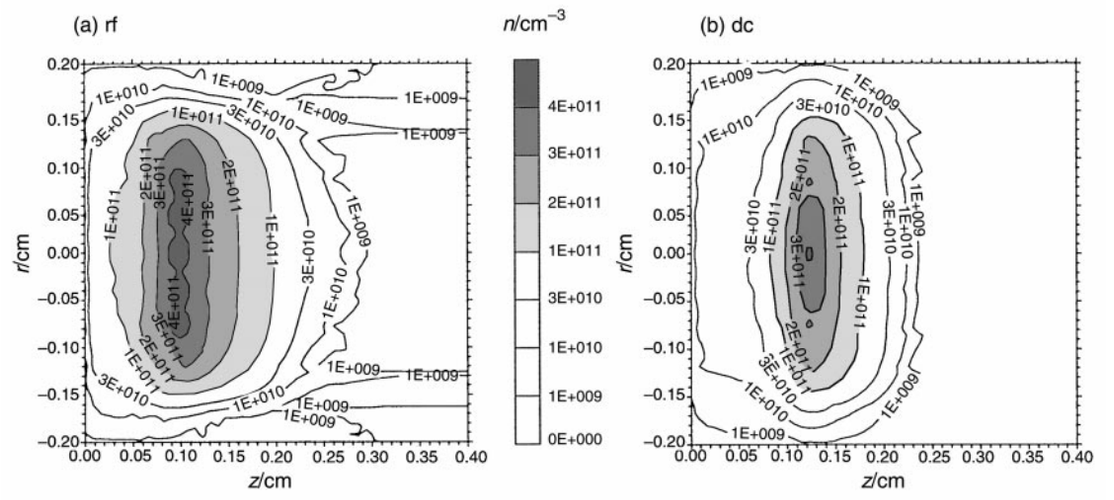

Fig. 9 Calculated two-dimensional density profiles of the copper Cu^+ ions, in the rf case (a) and the dc case (b). Only the first 4 mm from the electrode are shown. Reprinted from ref. 12, with permission of Elsevier Science.

The latter is also illustrated in Fig. 12, which presents the ionization rate, integrated over the entire discharge volume, as a function of time in the rf cycle. It is clear (upper part of the figure) that most of the rf ionization is due to fluid electrons (α-ionization). The latter is especially important around $\omega t = \pi/2$, as was expected already from the broad maximum in Fig. 11. Also shown for comparison is the dc ionization rate, integrated over the entire discharge volume. It is somewhat higher than the rf γ-ionization, but clearly lower than the rf α-ionization, as was illustrated already in Fig. 11. The lower part of Fig. 12 shows the ionization rate due to fast argon ions and atoms, both in the rf mode and the dc mode. It appears that these processes occur at a similar rate in both operation modes, when averaged over time. The cross sections of argon ion and atom impact ionization start to rise only for energies above several 100 eV. Since the argon ions and atoms can only reach high energies adjacent to the rf electrode or cathode (where they have gained energy from the high electric field in the sheath), these processes occur only in this region. Integrated over the entire rf discharge, they are, therefore, of minor importance compared to electron impact ionization (see the left axis of upper and lower part of Fig. 12). We calculated relative contributions for electron, argon ion and argon atom impact ionization of about 95%, 1% and 4%, respectively, in the rf case, and about 89%, 2% and 9%, respectively, in the dc case. The reason that electron impact ionization is even more significant in the rf case is of course due to the dominant role of α-ionization.

3.5 Information about sputtering at the rf electrode or cathode

The model network is also able to calculate the amount of sputtering at the rf electrode/cathode, based on the flux energy distributions of the argon ions, fast argon atoms and copper ions calculated with the Monte Carlo models, and on an empirical formula for the sputtering yield as a function of the bombarding energy. Fig. 13 illustrates the calculated net sputtering flux in the rf mode (as a function of time in the rf cycle) and in the dc mode, integrated over the entire electrode area ($J_{\mathrm{sput,net}}$). It appears that the net sputtering flux varies between $2\text{–}4 \times 10^{17}\ \mathrm{s}^{-1}$ for the rf mode, and is in the order of $2 \times 10^{17}\ \mathrm{s}^{-1}$ for the dc mode.

It should be mentioned that the "net" sputtering flux is the result of the total sputtering flux, calculated in the way mentioned above, minus the flux of redeposited copper atoms onto the electrode. The latter can be quite high, so that the net sputtering flux is only about 30–40% of the total sputtering flux. It is the net sputtering flux which gives rise to the erosion rate, by:[22]

$$ER = j_{\mathrm{sput,net}} \frac{M}{N_{\mathrm{A}} \rho}$$

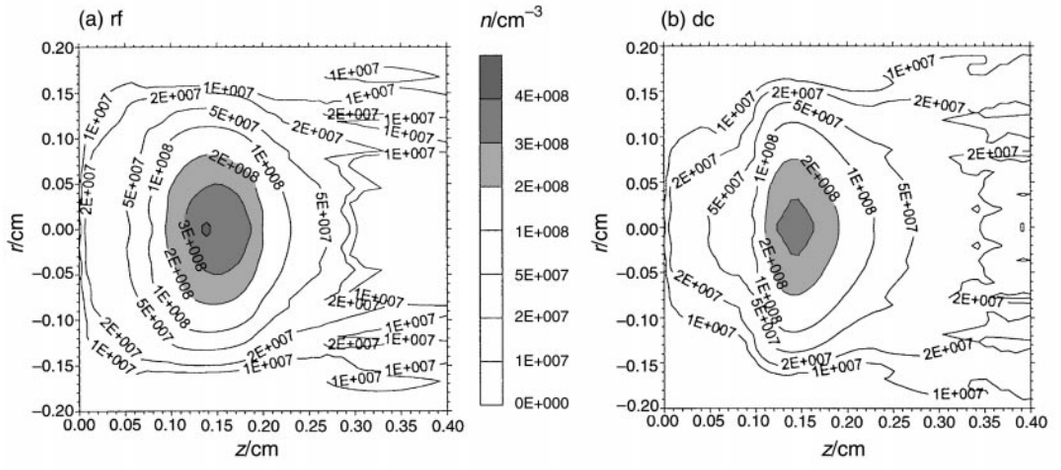

Fig. 10 Calculated two-dimensional density profiles of the Cu^{2+} ions, in the rf case (a) and the dc case (b). Only the first 4 mm from the electrode are shown. Reprinted from ref. 12, with permission of Elsevier Science.

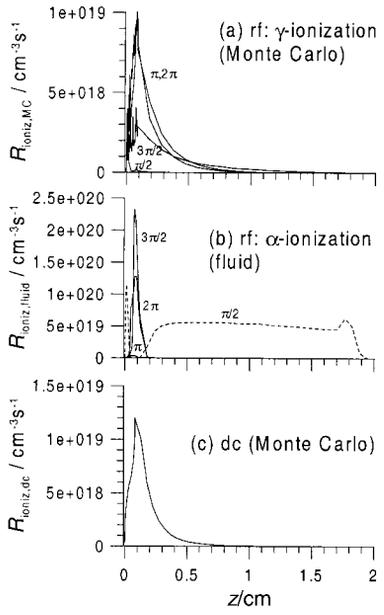

Fig. 11 Calculated one-dimensional electron impact ionization rates: (a) rf γ-ionization calculated with the Monte Carlo model, at four different times in the rf cycle; (b) rf α-ionization calculated with the fluid model, at four different times in the rf cycle; (c) dc ionization, calculated with the Monte Carlo model.

ER is the erosion rate (in cm s^{-1}), $j_{\text{sput, net}}$ is the net sputtering flux per unit area [in cm^{-2} s^{-1}; *i.e.*, $j_{\text{sput,net}} = J_{\text{sput,net}}$ (s^{-1})/ electrode area (cm^2)], *M* and ρ are the atomic weight (in g mol^{-1}) and density of the sample material [$\rho_{Cu} = 8.92$ g cm^{-3} (ref. 23)], and N_A is Avogadro's number.

Averaged over time in the rf cycle, the net sputtering flux ($J_{\text{sput,net}}$) is about 2.7×10^{17} s^{-1} (see Fig. 13) over the entire electrode area. For an anode diameter of 4 mm, the electrode area is about 0.126 cm^2. Hence, the net sputtering flux per unit area ($j_{\text{sput,net}}$) is about 2.1×10^{18} cm^{-2} s^{-1}, which corresponds to an erosion rate of about 0.253 μm s^{-1}. Experimentally, a value of 1 μm in 8 s was measured.[13] Hence, our calculated value (*i.e.*, ≈2.0 μm in 8 s) is higher, but still in the correct order of magnitude. In the dc case, the net sputtering flux, divided by the cathode area (=$j_{\text{sput,net}}$), was about 1.6×10^{18} cm^{-2} s^{-1}. This corresponds to an erosion rate of about 0.19 μm s^{-1}. The experimental value was 1 μm in 9 s;[13] hence our predicted value (*i.e.*, ≈1.7 μm in 9 s) is again higher. It can, however, be concluded that, although both calculated values are somewhat higher than the corresponding experimental data (in fact, we are already quite satisfied with this discrepancy of only a factor of 2), the calculated relative

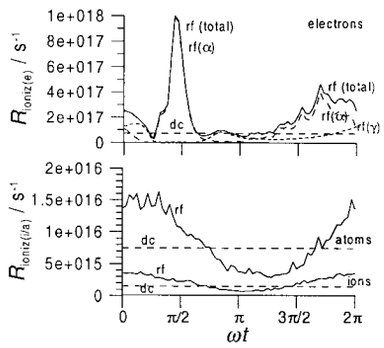

Fig. 12 Calculated ionization, integrated over the entire cell volume, in the rf case as a function of time in the rf cycle (solid lines) and in the dc case (dashed lines). Upper part: electron impact ionization (in the rf case: α, γ and the total ionization) and lower part: fast argon ion and atom impact ionization.

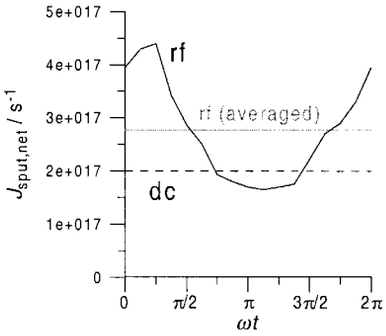

Fig. 13 Calculated net sputtering flux in the rf case, as a function of time in the rf cycle (black solid line) and time-averaged value (grey solid line), and in the dc case (broken line). Reprinted from ref. 12, with permission of Elsevier Science.

difference between rf and dc erosion rates is in reasonable agreement with the experimental observations of Hoffmann.[13]

Finally, the relative contributions to the sputtering of the different plasma species bombarding the electrode are calculated. The fast argon atoms appear to play the dominant role in the sputtering process, both in the rf and dc mode, with a relative contribution of 69.5% (rf) and 68.8% (dc), because the argon atom flux hitting the electrode is much higher than the argon and copper ion fluxes. However, the argon and copper ion energies bombarding the electrode are higher than the atom energy, and since the sputtering increases with bombarding energy, the argon and copper ions play also a non-negligible role in the sputtering process. Their contributions were calculated to be about 18.3% (rf) and 19% (dc) for the argon ions, and about 12.2% in both operation modes for the copper ions (called "self-sputtering").

3.6 Optical emission intensities

From the level populations of the excited argon atoms, copper atoms and ions calculated in the collisional–radiative models (see above), the optical emission intensities of spectral lines can be calculated, when multiplying the populations with the Einstein transition probabilities for radiative decay.

Fig. 14 illustrates the calculated optical emission spectrum of the argon atoms, both for the dc and the rf mode, integrated along the cell axis as a function of distance from the electrode, to simulate end-on observation. The spectrum contains 605 argon atom lines. The rf spectrum was found to be nearly constant during the rf cycle. For the dc discharge, this

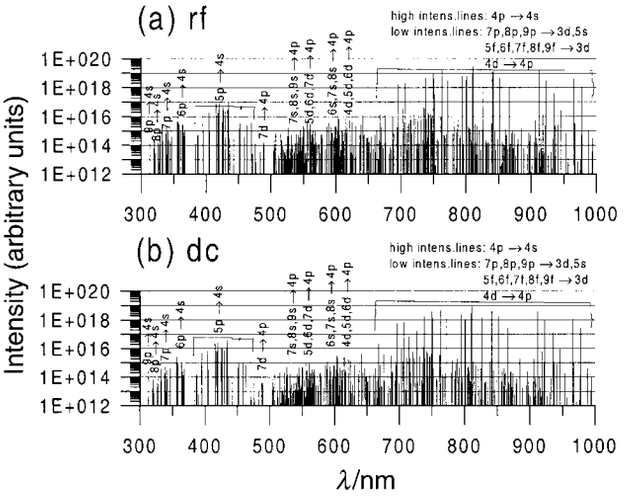

Fig. 14 Calculated argon atomic optical emission spectrum in end-on observations, in the rf case (a) and the dc case (b). Reprinted from ref. 9, with permission of Elsevier Science.

calculated spectrum has been checked against experimental data found in the literature in a previous paper, for somewhat different discharge conditions,[24] and satisfactory agreement has been reached. For the rf discharge, and for the comparison between the two operation modes, we intend to compare the calculations with experimental data at exactly the same conditions in the near future, as soon as the experimental data become available.

The spectra are presented on a semi-logarithmic plot, in order to show the large number of lines. It is, however, obvious that the region of 700–1000 nm is characterized by the most intense lines, *i.e.*, the so-called "red lines", corresponding to 4p–4s transitions. Furthermore, the region of 380–470 nm contains also rather strong lines, the so-called "blue lines", corresponding to 5p–4s transitions. When comparing the rf and dc spectra, it appears that the dc lines are somewhat less intense than the rf lines. However, the difference is less than a factor of about 2, so that we can conclude that our model calculations predict, for the same power levels, similar argon optical emission spectra in the rf and dc mode. This will have to be checked in the near future by comparing with experimental data, when available.

The optical emission spectrum of the copper atomic and ionic lines is presented in Fig. 15, for both the rf case (constant during the entire rf cycle) and the dc discharge, again integrated in the axial direction to simulate end-on observation. The intensities of 103 copper atomic and ionic lines are calculated. However, the spectrum might well contain more lines, originating from levels which were not considered in our collisional–radiative model (because no cross section data were available for them). Nevertheless, the most intense lines are probably all included in our calculated spectrum. When comparing the rf and dc spectra, it appears that the dc optical emission intensities are somewhat lower than the corresponding rf intensities. This seems to be especially the case for the atomic lines (*i.e.*, the dc values were found to be about one order of magnitude lower), whereas the ionic lines showed only a difference of 10–20%. Indeed, we found, in ref. 12, that the dc copper atomic level populations were clearly lower than the rf values, whereas the ionic levels were almost of the same magnitude. Experimentally, the Cu intensities were found to be about 10% lower in the dc case compared to the rf case.[13] Hence, this is apparently in good agreement with our calculated differences for the ionic lines, but the differences we calculated for the atomic lines seem to be somewhat too high. In general, however, both the rf and dc spectra have a very similar outlook. A detailed comparison with experiment, concerning both dc and rf spectra, is planned for the near future.

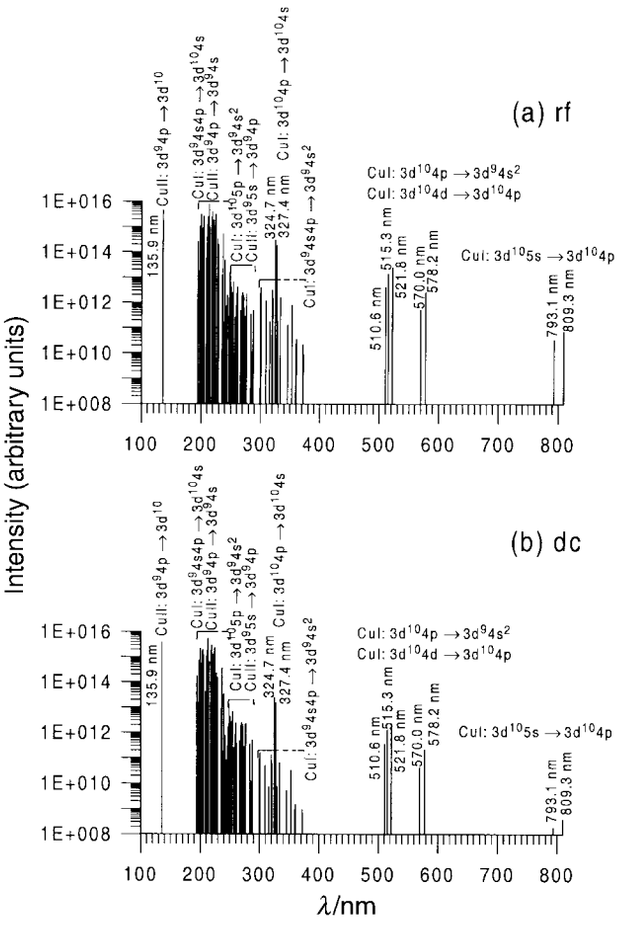

Fig. 15 Calculated copper atomic and ionic optical emission spectrum in end-on observations, in the rf case (a) and the dc case (b).

4 Conclusion

A hybrid two-dimensional modeling network has been developed for dc and rf glow discharges in argon with a copper cathode. The network consists of several sub-models (Monte Carlo, fluid and collisional–radiative models) to describe the behavior of electrons, argon ions, fast argon atoms, argon atoms in various excited levels, and copper atoms and ions, both in the ground state and in various excited levels. Typical results of the models comprise the electrical characteristics (voltage, current, power, potential and electric field distributions), the densities, fluxes and energies of the various plasma species, information about collisions in the plasma and about sputtering at the rf electrode or cathode, and optical emission intensities. Some of these results are presented and compared between the two operation modes. It appears that, for the same values of electrical power and pressure, the rf discharge requires lower voltages than the dc discharge. The reason for this is the more efficient ionization in the rf mode. Indeed, not only so-called γ-ionization (*i.e.*, due to electrons emitted from the electrode or created in the sheath, and accelerated by the strong electric field, as in the dc mode) plays a role, but the slow electrons in the plasma can also become heated again in the oscillating rf electric field, and give rise to so-called α-ionization. Also, the argon ion and electron densities, and, to a less extent, the argon excited atom densities are slightly higher in the rf mode than in the dc mode, and they drop more slowly as a function of distance from the rf electrode. Hence, it appears that, in the rf case, the discharge cell is more filled with plasma than in the dc case. The sputtered copper atom and ion densities are, however, calculated to be more or less comparable in both operation modes. The sputtering at the rf electrode or cathode has also been calculated, and the obtained erosion rates were found to be in acceptable agreement with experimental data, both the absolute values and the relative values between dc and rf mode (dc values slightly lower than rf values). Finally, the optical emission spectra of argon and copper have been calculated for both operation modes, and the rf spectral intensities were found to be slightly higher than the corresponding dc intensities, which also agrees with observations.

Hence, our calculation results are found to be in reasonable agreement with experimental data, when available, *i.e.*, erosion rates, optical emission intensities, as well as the rf voltage as a function of time, the dc bias voltage, and the dc voltage, when pressure and power are given. In the near future, we plan to perform a more detailed comparison with experimental data, in the framework of the EC Thematic Network on Glow Discharge Spectroscopies.

Acknowledgements

A. Bogaerts is indebted to the Flemish Fund for Scientific Research (FWO) for financial support. This research is also sponsored by the Federal Services for Scientific, Technical and Cultural Affairs of the Prime Minister's Office (DWTC/SSTC) through IUAP-IV (Conv. P4/10). Finally, we wish to thank V. Hoffmann (IFW, Dresden) for supplying the experimental data and for the many interesting discussions.

References

1 A. Bogaerts and R. Gijbels, *J. Anal. At. Spectrom.*, 1998, **13**, 945.
2 A. Bogaerts, M. van Straaten and R. Gijbels, *Spectrochim. Acta, Part B*, 1995, **50**, 179.
3 A. Bogaerts, R. Gijbels and W. Goedheer, *Jpn. J. Appl. Phys.*, 1999, **38**, 4404.
4 A. Bogaerts, M. Yan, R. Gijbels and W. Goedheer, *J. Appl. Phys.*, 1999, **86**, 2990.
5 A. Bogaerts, R. Gijbels and W. Goedheer, *J. Appl. Phys.*, 1995, **78**, 2233.
6 A. Bogaerts and R. Gijbels, *J. Appl. Phys.*, 1995, **78**, 6427.
7 A. Bogaerts and R. Gijbels, *IEEE Trans. Plasma Sci.*, 1999, **27**, 1406.
8 A. Bogaerts, R. Gijbels and J. Vlcek, *J. Appl. Phys.*, 1998, **84**, 121.
9 A. Bogaerts and R. Gijbels, *Spectrochim. Acta, Part B*, 2000, in the press.
10 A. Bogaerts, M. van Straaten and R. Gijbels, *J. Appl. Phys.*, 1995, **77**, 1868.
11 A. Bogaerts, R. Gijbels and R. J. Carman, *Spectrochim. Acta, Part B*, 1998, **53**, 1679.
12 A. Bogaerts and R. Gijbels, *Spectrochim. Acta, Part B*, 2000, in the press.
13 V. Hoffmann, private communication.
14 D. B. Graves and K. F. Jensen, *IEEE Trans. Plasma Sci.*, 1986, **14**, 78.
15 D. Passchier, Ph.D. Thesis, University of Utrecht, 1994.
16 V. Hoffmann, H.-J. Uhlemann, F. Präβler, K. Wetzig and D. Birus, *Fresenius' J. Anal. Chem.*, 1996, **355**, 826.
17 D. Fang and R. K. Marcus, *Spectrochim. Acta, Part B*, 1990, **45**, 1053.
18 D. Fang and R. K. Marcus, *Spectrochim. Acta, Part B*, 1991, **46**, 983.
19 Y. Ye and R. K. Marcus, *Spectrochim. Acta, Part B*, 1996, **51**, 509.
20 A. Bogaerts, R. Gijbels and W. J. Goedheer, *Anal. Chem.*, 1996, **68**, 2296.
21 A. Bogaerts and R. Gijbels, *Spectrochim. Acta, Part B*, 1998, **53**, 437.
22 A. Bogaerts and R. Gijbels, *Spectrochim. Acta, Part B*, 1997, **52**, 765.
23 R. C. Weast and M. J. Astle, *CRC Handbook of Chemistry and Physics*, CRC Press, Boca Raton, FL, 1982–1983, 63rd edn.
24 A. Bogaerts, R. Gijbels and J. Vlcek, *Spectrochim. Acta, Part B*, 1998, **53**, 1517.